Geologica Acta, Vol.9, Nos 3-4, September-December 2011, 389-405
DOI: 10.1344/105.000001662
Available online at www.geologica-acta.com

geologica acta

Serpentinites and serpentinites within a fossil subduction channel: La Corea mélange, eastern Cuba

I.F. BLANCO-QUINTERO [1] [*] **J.A. PROENZA** [2] **A. GARCÍA-CASCO** [1] [3] **E. TAULER** [2] **S. GALÍ** [2]

[1] **Departamento de Mineralogía y Petrología, Universidad de Granada**
Fuentenueva s/n, 18002-Granada, Spain

[2] **Departament de Cristal·lografia, Mineralogia i Dipòsits Minerals, Facultat de Geologia, Universitat de Barcelona (UB)**
Martí i Franquès s/n, 08028-Barcelona, Spain

[3] **Instituto Andaluz de Ciencias de la Tierra (CSIC-UGR)**
Fuentenueva s/n, 18002-Granada, Spain

*Corresponding author. E-mail: blanco@ugr.es. Tel.: +34 958 246 613; Fax: +34 958 243 368

ABSTRACT

A variety of metaultramafic (serpentinite) rocks in La Corea mélange, Sierra de Cristal, eastern Cuba, show differences in chemical, textural and mineralogical characteristics demonstrating a variety of protoliths. The mélange originated during the Cretaceous as part of the subduction channel associated with the Caribbean island arc. This mélange contains high pressure blocks in a serpentinite matrix and occurs at the base of the large tabular Mayarí-Cristal ophiolite. Two principal groups of serpentinites have been identified in the mélange: a) antigorite serpentinite, mainly composed of antigorite and b) antigorite-lizardite serpentinite, composed of mixtures of antigorite and lizardite and bearing distinctive porphyroblasts of diopsidic clinopyroxene. Antigorite serpentinites are closely related to tectonic blocks of amphibolite (representing subducted MORB) and constitute deep fragments of the serpentinitic subduction channel formed during hydration of the mantle wedge. The composition of the antigorite-lizardite serpentinites and the presence of clinopyroxene porphyroblasts in this type of rock suggest that abyssal lherzolite protoliths transformed into serpentinite before and during incorporation (as tectonic blocks) in the shallow part of the subduction channel. Although the studied rocks have different origin, mineralogical compositions and textures, they display similar PGE compositions, suggesting that these elements experienced no significant redistribution during metamorphism. Both types of serpentinites were exposed together in the La Corea mélange during the Late Cretaceous, during obduction of the overriding Mayarí-Baracoa ophiolitic belt that led to exhumation of the subduction channel (mélange).

KEYWORDS | **Serpentinite. Subduction Channel. La Corea Mélange. Cuba. Caribbean.**

INTRODUCTION

Ophiolite-related ultramafic rocks, commonly strongly serpentinized, appear along the margins of Caribbean Plate, being most abundant in the northern edge, principally in Cuba (Lewis et al., 2006a and references therein). These ultramafic rocks represent fragments of oceanic and sub-arc lithospheric mantle that were altered, completely or partly, to serpentinites by fluids during their evolution and accretion to the Caribbean orogenic belt. In Cuba, these ophiolitic bodies are related to serpentinite-matrix mélanges containing high-pressure (HP) blocks of different origin and composition (e.g. García-Casco et al., 2006, and references therein). These mélanges can be interpreted as the exhumed subduction channel of the Caribbean subduction zone (e.g. Gerya et al., 2002).

Two serpentinite-matrix mélanges have been documented in eastern Cuba, 100km apart (Fig. 1): La Corea and Sierra del Convento mélanges (Somin and Millán, 1981; García-Casco et al., 2006). The origin and evolution of the HP (garnet-epidote amphibolite and blueschists) blocks from both mélanges has been studied by García-Casco et al. (2006, 2008a), Lázaro and García-Casco (2008), Lázaro et al. (2009) and Blanco-Quintero et al. (2010). However, no detailed petrological and geochemical studies have been performed to characterize mélange serpentinites.

The serpentinitic rocks present in La Corea mélange have mineralogical and geochemical characteristics that indicate varied P-T conditions of formation and variable protoliths. The mélange formed during Cretaceous times in response to SW-dipping subduction beneath the northern Caribbean plate. In this paper we provide new petrological and geochemical data of representative serpentinite samples from the La Corea mélange in order to evaluate its nature, the environments of formation of serpentinites, and the implications for tectonic interactions between the Caribbean and North American plates.

GEOLOGICAL SETTING

The Cuban fold and thrust belt formed during Mesozoic to middle Eocene times in the active Caribbean-North American plate margin. It is now accreted to the southern margin of the North American plate (Fig. 1A). The Cuban orogenic belt includes several imbricated geologic complexes, including fragments of the Caribean terrane (Cangre, Pinos, Escambray and Asunción metamorphic complexes), the Bahamas platform (Cayo Coco, Remedios, Camajuaní belts), the margin of the Maya block (the Guaniguanico terrane), two different volcanic arc complexes of Cretaceous and Paleogene ages respectively, ophiolite bodies forming the northern and eastern ophiolite belts, and syn- and post-orogenic sedimentary basins (Iturralde-Vinent, 1998; Iturralde-Vinent et al., 2006, 2008; García-Casco et al., 2008b).

The most important tectonic units in northeastern Cuba are the ophiolites and the Cretaceous volcanic arc (Fig. 1B). Systematically the Cretaceous volcanic arc appears tectonically below the ophiolites. The Cretaceous volcanic arc units contain a number of basic to acid volcanic units having distinct island arc tholeiitic, boninitic and calc-alkaline signatures (Iturralde-Vinent et al., 2006; Proenza et al., 2006; Marchesi et al., 2007). The age of these formations has been paleontologically estimated to range from early Cretaceous (Aptian-Albian) to late Cretaceous (Campanian) times (Iturralde-Vinent, et al., 2006). The Purial volcanic complex, located in the southern part of the region, is metamorphosed to the greenschist and blueschist facies (Boiteau et al., 1972; Cobiella et al., 1977; Somin and Millán, 1981; Millán et al., 1985).

The ophiolite complex is represented by the Mayarí-Baracoa Ophiolitic Belt. This belt is constituted strongly deformed and faulted mafic-ultramafic thrust sheets and by the overriding Cretaceous volcanic arc and Maastrichtian-Danian olistostromic formations related to obduction (Iturralde-Vinent et al., 2006). The direction of tectonic transport is NNE (Nuñez-Cambra et al., 2004), as expected for a SW-dipping subduction zone. The Mayarí-Baracoa Ophiolitic Belt shows supra-subduction geochemical signatures (Proenza et al., 1999, 2006; Gervilla et al., 2005; Marchesi et al., 2006, 2007), and include the Mayarí-Cristal massif to the west and the Moa-Baracoa massif to the east (Fig. 1B). According to Marchesi et al. (2006) Mayarí-Baracoa Ophiolitic Belt is composed of highly depleted peridotites and cumulate gabbroic rocks. Mayarí-Baracoa Ophiolitic Belt Peridotites were highly altered (serpentinized) by seawater during the oceanic stage (Proenza et al. 2003). The Moa-Baracoa massif represents MORB-like back-arc lithosphere while Mayarí-Cristal is transitional (MORB to IAT) mantle located closer to the paleo-volcanic arc (Marchesi et al., 2006).

The Mayarí-Cristal massif is > 5km thick and is made up of harzburgite tectonite hosting minor subconcordant dunite layers and subordinate discordant microgabbro-diabase dykes. Some authors have described a sheeted-dyke complex in the northwestern part of the massif (e.g., Fonseca et al., 1985), but Marchesi et al. (2006) argue that this is a subvolcanic complex made up of massive microgabbros in tectonic contact with harzburgite tectonites. The Mayarí-Cristal harzburgites display porphyroclastic texture. They are clinopiroxene and generally have higher orthopiroxene/olivine ratios than the Moa-Baracoa harzburgites (Marchesi et al., 2006). The harzburgite tectonites show a NE–SW oriented foliation dipping NW (Marchesi et al., 2006), and the contact with the dunites is sharp.

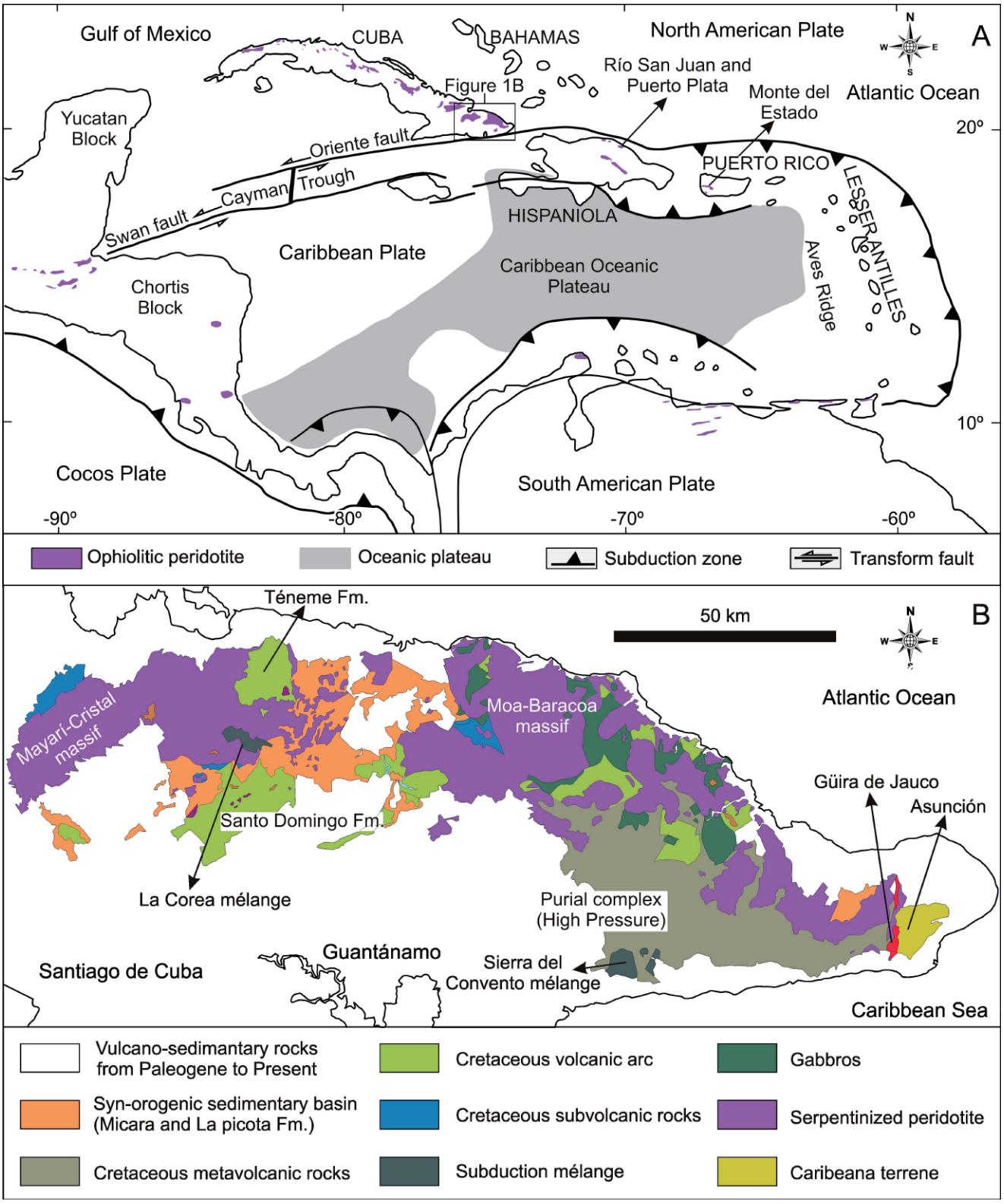

FIGURE 1 | **A) Plate tectonic configuration of the Caribbean region, including ophiolitic bodies. B) General geologic map of eastern Cuba showing the main geological units.**

The La Corea mélange, containing high pressure exotic blocks, is located in tectonic contact with ultramafic rocks of the Mayarí-Cristal massif (Fig. 1B). The tectonic position of La Corea mélange suggests that this metamorphic complex is overridden by the ophiolites, and that both override the Cretaceous volcanic arc units and the Maastrichtian-Danian olistostromic synorogenic rocks of Micara and La Picota formations. The mélange is made up of exotic blocks of diverse origin and composition (garnet-amphibolite, blueschist and greenschist are dominant) within a serpentinite matrix. Metamorphism of the amphibolites evolved under high- to medium-pressure (ca. 700ºC, 15kbar) related to a hot subduction environment from high- to low-temperature following counterclockwise P-T paths related to exhumation in the subduction channel (Blanco-Quintero et al., 2010).

The most abundant rock type is a MORB-derived epidote ± garnet amphibolite that contains a peak metamorphic assemblage made of pargasite, epidote, titanite, rutile ± quartz ± garnet ± phengite ± plagioclase and accessory apatite (Blanco-Quintero et al., 2010). The amphibolite blocks are massive to banded and of metric-size. Metaleucocratic rocks (tonalites-trondhjemites) occur as veins and blocks intimately associated with the amphibolites. The tonalites-trondhjemites are medium- to coarse-grained, including pegmatitic varieties, and are composed of quartz, albite-oligoclase, epidote, ± calcic amphibole (pargasite-actinolite) ± muscovite-phengite. These rocks formed after partial melting of subducted MORB amphibolites at 700ºC, 15kbar (Blanco-Quintero et al., 2010). Other tectonic blocks within the mélange include schists of variable composition and origin. Ultramafic rocks are mainly massive to foliated antigoritite forming the mélange matrix. Occasionally massive antigoritite blocks are included as boudins in strongly foliated antigorite rocks. In addition, blocks of serpentinite with bastite crystals are surrounded by foliated antigoritite. Masses of tremolite-actinolite rocks (composed of > 95% radial and tabular amphibole) and other metasomatic products of mafic and ultramafic composition are present.

Available isotopic data (Adamovich and Chejovich, 1964; Somin and Millán, 1981) indicates that the subduction channel mélange began to form ca. 110Ma. Final exhumation of the mélange occurred during the initial thrusting of the ophiolitic and volcanic arc units in the Late Campanian-Maastrichtian (Iturralde-Vinent et al., 2006; Lázaro et al., 2009).

In this study we characterize serpentinite rocks from the La Corea mélange, including antigorite serpentinites (5 samples: LC-G-4, LC-M-17, LC-55, LC-56 and LC-58) and antigorite-lizardite serpentinites (3 samples: LC-66, LC-88 and LC-97).

ANALYTICAL TECNIQUES

Powder X-ray diffraction (XRD) data were collected with a Panalytical X'Pert PRO MPD X-ray diffractometer with monochromatized incident Cu Kα1 radiation at 45keV and 40mA, and equipped with a x'Celerator detector of active length of 2.112º at the Serveis Cientificotècnics of the Universitat de Barcelona (Spain). The patterns were obtained by scanning powders from 4°-80° 2θ on samples crushed in an agate mortar to a particle size < 20μm. Quantitative mineral phase analyses of samples were obtained by full profile Rietveld refinement using powder diffraction data. The mineral identification software used was TOPAS V3.0.

Mineral compositions were obtained by electron microprobe using a wavelength dispersive X-ray spectometry (WDS-CAMECA SX 50) at the Serveis Cientificotècnics of the Universitat de Barcelona (Spain). Excitation voltage was 20kV and beam current 15nA. Most elements were measured with a counting time of 10s, except for Ni (30s). The chemical data for serpentine, clinopyroxene, talc and chlorite compositions were normalized to 14, 6, 22 and 28 oxygens respectively, and $Fe_{total} = Fe^{2+}$. Garnet composition was normalized to 8 cations and 12 oxygens, and Fe^{3+} was estimated by stoichiometry. The atomic concentration of elements per formula unit is abbreviated apfu. The Mg number of minerals ($Mg/(Mg+Fe^{2+})$) is expressed as Mg#. Mineral abbreviations are after Kretz (1983).

Major element compositions were determined on glass beads, made of 0.6g of powdered sample diluted in 6g of $Li_2B_4O_7$, by a PHILIPS Magix Pro (PW-2440) X-ray fluorescence (XRF) equipment (University of Granada, Centro de Instrumentación Científica, CIC). Precision was better than ±1.5% for a concentration of ≥10 wt% and ±2% for a concentration <10 wt%. Platinum-group element concentrations were determined by isotopic dilution using Inductively Coupled Plasma-Mass spectometry (ICP-MS) after nickel sulfide fire assay, in the Genalysis Laboratory Services Pty. Ltd. at Maddington (Western Australia) following the method described by Chan and Finch (2001). The detection limits were 1 ppb for Rh, and 2 ppb for Os, Ir, Ru, Pt, Pd.

PETROGRAPHY AND SERPENTINE MINERALS

On the basis of mineral assemblages and textures of metaultramafic rocks, two principal groups of serpentinite have been identified (Figs. 2 and 3): i) antigorite serpentinite and ii) antigorite-lizardite serpentinite.

Antigorite serpentinites (group I) consist mainly of antigorite (up to 94%), with minor talc-magnesite-dolomite (Fig. 2A-D, Fig. 3A). However, some samples (e.g. LC-55)

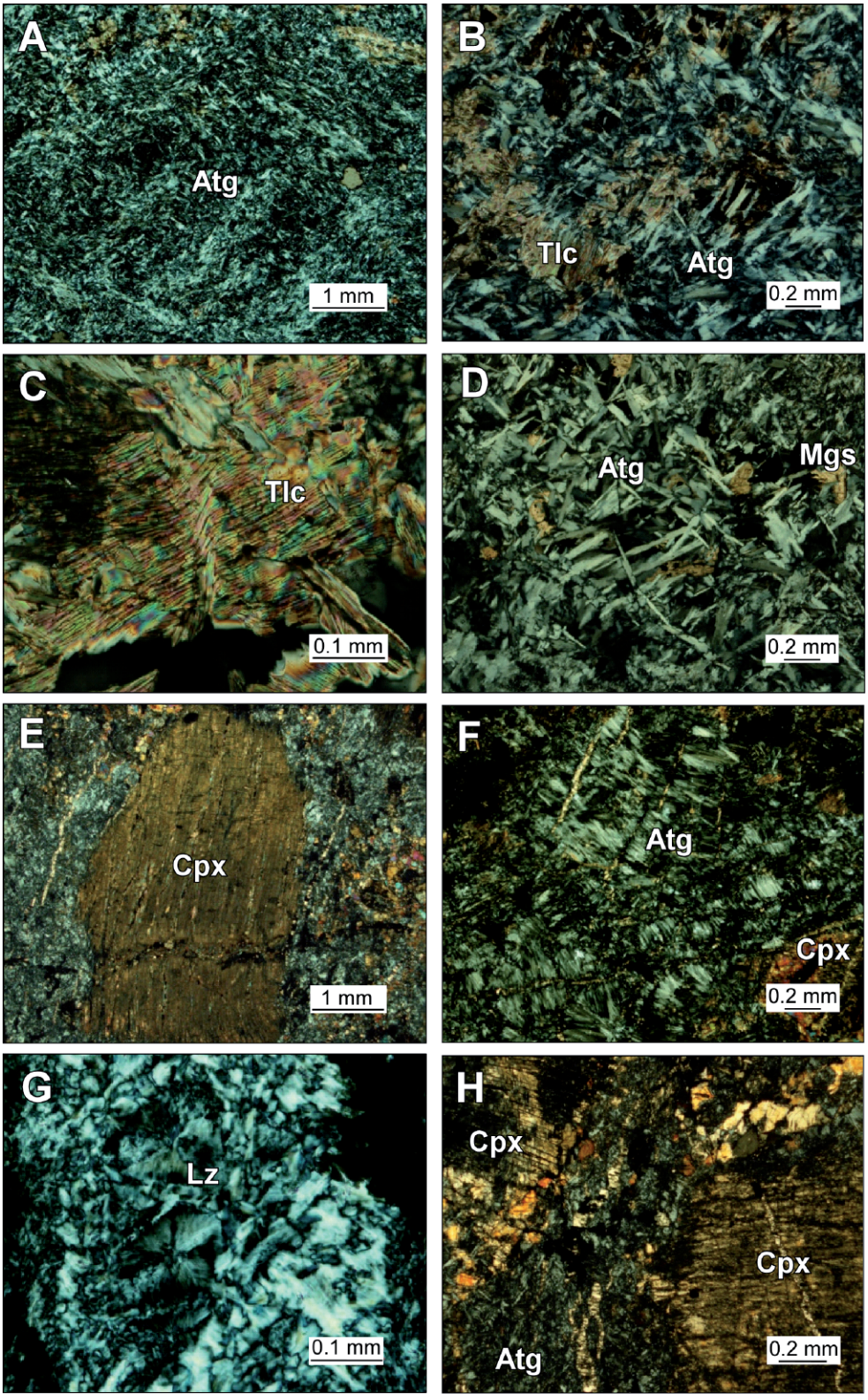

FIGURE 2 | **Cross-polarized light photographs of antigorite serpentinite (A to D) and antigorite-lizardite serpentinite (E to H). A) Nonpseudomorphic interpenetrating texture typical of antigorite. B) Talc-bearing antigorite serpentinite. Antigorite is partially replaced by talc. C) Kinking of talc in talc-bearing antigorite serpentinites. D) Detail of antigorite interpenetrating texture. Antigorite grains are partially replaced by magnesite and minor dolomite. E) Porphyroclastic texture showing clinopyroxene (diopside). F) Clinopyroxene partly replaced by ribbons of antigorite. Antigorite is a product of recrystallization of lizardite; G) Type-1 lizardite hourglass texture, showing the optical uniformity of lizardite across the mesh cell; H) Porphyroblastic and fine grained diopsidic clinopyroxene.**

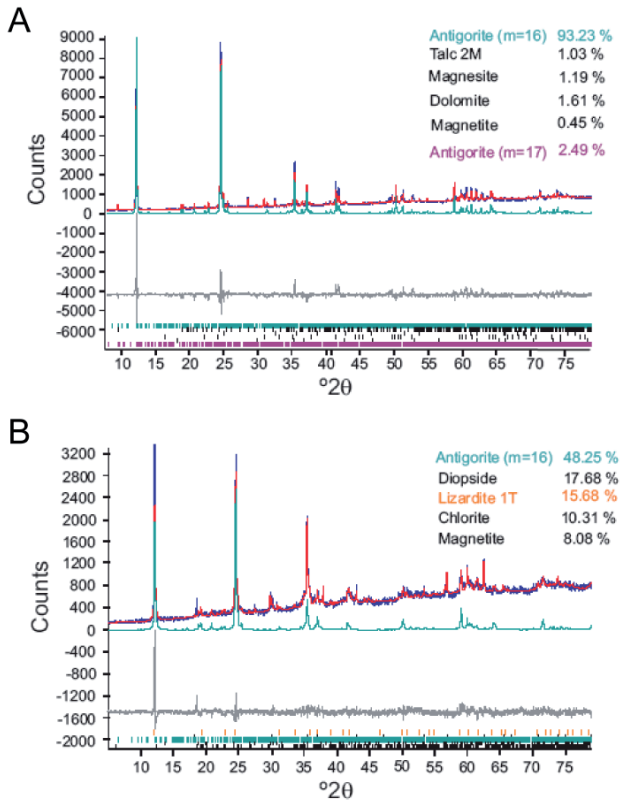

FIGURE 3 | **XRD profile refinements of representative samples of A) antigorite- (LC-58) and B) antigorite-lizardite- (LC-88) serpentinites showing experimental (blue), calculated (red), calculated antigorite (turquoise), and difference (grey) profiles. The Bragg positions for all identified mineral phases are indicated at the base of the diagram.**

contain abundant talc (Fig. 2C). Kinking of talc crystals, typical of plastic deformation (Escartín et al., 2008), is common. Antigorite grains are partially replaced by magnesite and minor dolomite (Fig. 2D). Systematically, the relicts of Cr-spinel grains are altered to ferrian chromite and magnetite, and chlorite appears forming rims around altered spinel.

Serpentinites of group I are characterized by non-pseudomorphic textures, typically showing the characteristic interpenetrating needles of antigorite (Fig. 2A, B, D; O'Hanley, 1996).

The antigorite-lizardite serpentinites (group II) contain the mineral assemblage antigorite - lizardite - diopsidic clinopyroxene - chlorite - magnetite - ferrian chromite ± brucite. They are characterized by porphyroblastic texture, showing relicts of bastitized clinopyroxene porphyroblasts up to 8mm in size (Fig. 2E). The dominant serpentine mineral is antigorite (Fig. 2F), but lizardite has been identified in thin section and by XRD (Figs 2G, 3B). Clinopyroxene porphyroblasts are partly overgrown/replaced by fine-grained clinopyroxene, antigorite, chlorite and magnetite (Fig. 2H). The hedenbergite component of clinopyroxene was oxidized to magnetite, which is mainly associated with serpentine along exfoliation planes and the rims of the grains of clinopyroxene. Primary Cr-spinels were not found; only their alteration products, ferrian chromite and newly formed magnetite, are present. In addition, chlorite forms rims around altered spinel. Andradite garnet is present in veins crosscutting the serpentine matrix. It is colourless and forms granular aggregates.

In general, antigorite-lizardite serpentinites preserve pseudomorphic textures (Wicks and Whittaker, 1977; O'Hanley, 1996): i) bastites after clinopyroxene and ii) hourglass textures (Figure 2G). Theses textures can be interpreted as the result of low grade metamorphism (i.e. ocean floor metamorphism).

Serpentine minerals

In order to identify and quantify the amount of serpentine minerals (chrysotile, lizardite and antigorite) and the lattice parameters of these structures, the observed random X-ray powder diffraction profile was simulated using several structural models of antigorite polymorphs (Rietveld method). Commonly, antigorite in serpentinites forms a polysomatic series of sheet silicates of variable structure and composition (e.g. Mellini et al., 1987). The variation of *a* parameter is expressed in terms of *m*, which is the number of SiO_4 tetrahedra seen in a projection along [010] within a full wavelength of the modulated structure.

The calculated XRD profile of group I serpentinite (sample LC-58) agrees well with two serpentine polymorphs (Fig. 3A), one with antigorite polysome m=16 with 16 tetrahedra spanning a wavelength along the *a* axis as proposed by Capitani and Mellini (2006) and the other with antigorite polysome m=17 (Capitani and Mellini, 2004). The structure with m=16 resembles that of the m=17 polysome. In both, a continuous wavy tetrahedra sheet layer (linked to brucite-like layer) reverses polarity through sixfold and eightfold tetrahedra rings. The even number of tetrahedra in m=16, leads to symmetric half-waves, a periodic *b/2* shift involving the eightfold rings, and the doubling of a parameter. The result is a C monoclinic cell.

The antigorite with polysome m=16 yields the best fit for the most abundant in group I serpentinite (93.2wt%) and the fitted lattice parameters are: a=81.878(5), b=9.264(5), c=7.248(2) Å and β = 91.409(5)°, space group C2/m. The antigorite with m=17 is scarce, 2.5wt%, and the obtained parameters are: a=43.505(6), b=9.251(1), c=7.263(1) Å and β = 91.32(1)°, space group Pm. Other mineral phases present in the sample are: talc (1.0wt%), magnesite (1.2wt%), dolomite (1.6wt%) and magnetite (0.5wt%). Mellini et al. (1987) and Li et al. (2004) suggested that

m=17 is typical for antigorite formed under greenschist-facies conditions.

In group-II serpentinites (sample LC-88) the calculated profile agrees well with the antigorite polysome m=16 and lizardite 1T (Mellini and Viti, 1994) (Fig. 3B). Antigorite is the most abundant serpentine mineral (48.3wt%) with lattice parameters a=81.551(6), b=9.247(10), c=7.266(4) Å and β = 91.00(11)°. Lizardite is also abundant (15.7wt%), with lattice parameters a=5.322(2), c= 7.295 (6) Å and space group P31m. Other phases identified in this sample are: diopside (17.7wt%), clinochlore (10.3wt%), magnetite (8.1wt%) and minor brucite.

In summary, all investigated antigorites of the La Corea mélange presents polysome values with m=16. However, the variability of the refined a parameter in these samples is too low to permit correlation with the metamorphic grade as suggested by Mellini et al. (1987) and Li et al. (2004).

MINERAL CHEMISTRY

Serpentine

Serpentine from antigorite serpentinites have Si ranging 3.94 – 4.04 apfu, Mg = 4.94 – 5.08 apfu, Fe = 0.5 – 0.59 apfu, Cr < 0.05 apfu and Ni < 0.05 apfu (Table 1). In the ternary diagram Mg-Si-Fe (molar proportions, Fig. 4) the analyzed grains of serpentinite confirm with antigorite composition following D'Antonio and Kristensen (2004) classification. The Al contents are relatively high (0.21 – 0.30 apfu). High Al and Cr could produce highest stability in temperature for antigorite (Padrón-Navarta et al., 2010). The Mg # ratios are 0.89 – 0.91.

Serpentine from antigorite-lizardite serpentinites have Si = 3.94 – 4.03 apfu, Fe = 0.19 – 0.26 apfu, Mg = 5.34 – 5.41 apfu, Cr < 0.03 apfu and Ni < 0.03 apfu, showing relative high Al = 0.17 – 0.30 apfu (Table 2). In the ternary diagram Mg-Si-Fe (Fig. 4) most point analyses represent antigorite composition, although some points with less Si content indicate lizardite and/or chrysotile composition (D'Antonio and Kristensen, 2004). The Mg# (0.95 – 0.97) is higher than in the antigorite serpentinites. These higher values do not correlate with bulk rock composition, suggesting distinct P-T conditions of growth.

Clinopyroxene

The porphyroblasts of clinopyroxene present in antigorite-lizardite serpentinites are diopside (≈ En50 Wo49-50 Fs0; Morimoto et al., 1989; Table 3), with Si contents ranging 1.97 – 1.99 apfu, Mg = 0.96 – 1.03 apfu, Ca = 0.95 – 1.01 apfu, and very low Fe contents (< 0.05 apfu).

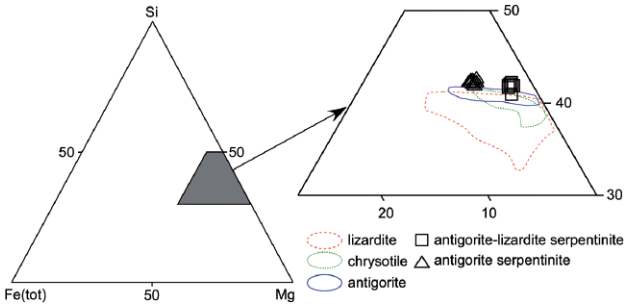

FIGURE 4 | **Ternary atomic Mg-Si-Fe diagram showing the chemical variability of serpentine minerals from La Corea mélange. The fields for lizardite, chrysotile and antigorite were compiled by D'Antonio and Kristensen (2004).**

TABLE 1 | **Representative analyses of serpentine from antigorite serpentinites (normalized to 10 O and 8 OH)**

Sample	LC-58	LC-58	LC-58	LC-58	LC-58	LC-55	LC-55	LC-55	LC-55	LC-55
SiO_2	42.81	43.01	42.46	43.16	42.46	41.84	41.58	42.04	41.54	41.91
TiO_2	0.02	0.04	0.03	0.03	0.03	0.04	0.02	0.03	0.02	0.03
Al_2O_3	1.86	2.31	2.20	2.07	1.88	2.49	2.66	2.47	2.46	2.24
Cr_2O_3	0.26	0.34	0.37	0.17	0.17	0.56	0.58	0.62	0.62	0.53
FeO_{total}	6.39	6.31	6.59	6.78	6.50	7.41	7.08	7.05	7.03	7.05
MnO	0.04	0.03	0.09	0.08	0.04	0.02	0.00	0.05	0.01	0.02
MgO	36.00	35.75	35.64	36.26	36.01	34.86	34.74	35.05	35.54	34.69
NiO	0.15	0.12	0.18	0.15	0.26	0.19	0.25	0.12	0.34	0.13
CaO	0.00	0.01	0.01	0.00	0.00	0.01	0.00	0.01	0.03	0.02
Total	87.53	87.92	87.57	88.70	87.35	87.42	86.91	87.44	87.59	86.62
Si	4.03	4.03	4.01	4.02	4.02	3.98	3.97	3.99	3.94	4.01
Ti	0.00	0.00	0.00	0.00	0.00	0.00	0.00	0.00	0.00	0.00
Al	0.21	0.26	0.24	0.23	0.21	0.28	0.30	0.28	0.27	0.25
Cr	0.02	0.03	0.03	0.01	0.01	0.04	0.04	0.05	0.05	0.04
Fe^{2+}	0.50	0.49	0.52	0.53	0.51	0.59	0.57	0.56	0.56	0.56
Mn	0.00	0.00	0.01	0.01	0.00	0.00	0.00	0.00	0.00	0.00
Mg	5.06	5.00	5.02	5.04	5.08	4.94	4.94	4.96	5.03	4.95
Ni	0.02	0.02	0.03	0.02	0.04	0.03	0.04	0.02	0.05	0.02
Ca	0.00	0.00	0.00	0.00	0.00	0.00	0.00	0.00	0.00	0.00
#Mg	0.91	0.91	0.91	0.91	0.91	0.89	0.90	0.90	0.90	0.90

TABLE 2 | **Representative analyses of serpentine from antigorite-lizardite serpentinites (normalized to 10 O and 8 OH)**

Sample	LC-88	LC-88	LC-88	LC-88	LC-66	LC-66	LC-66	LC-66
SiO_2	42.53	42.52	43.66	42.80	43.49	43.09	43.06	42.21
TiO_2	0.06	0.00	0.02	0.03	0.02	0.00	0.04	0.03
Al_2O_3	2.21	2.42	1.54	2.50	2.48	2.40	2.47	2.76
Cr_2O_3	0.31	0.29	0.18	0.25	0.38	0.45	0.35	0.07
FeO_{total}	2.95	2.75	2.83	3.23	2.80	2.50	2.49	3.34
MnO	0.14	0.07	0.10	0.06	0.09	0.14	0.19	0.07
MgO	38.86	38.47	39.23	38.67	39.10	39.41	38.72	38.43
NiO	0.07	0.12	0.20	0.17	0.16	0.12	0.13	0.00
CaO	0.01	0.33	0.00	0.01	0.00	0.02	0.01	0.29
Total	87.14	86.97	87.76	87.72	88.52	88.13	87.46	87.20
Si	3.97	3.97	4.03	3.97	3.98	3.97	3.99	3.94
Ti	0.00	0.00	0.00	0.00	0.00	0.00	0.00	0.00
Al	0.24	0.27	0.17	0.27	0.27	0.26	0.27	0.30
Cr	0.02	0.02	0.01	0.02	0.03	0.03	0.03	0.01
Fe^{2+}	0.23	0.21	0.22	0.25	0.21	0.19	0.19	0.26
Mn	0.01	0.01	0.01	0.00	0.01	0.01	0.01	0.01
Mg	5.40	5.36	5.40	5.34	5.34	5.41	5.35	5.35
Ni	0.01	0.02	0.03	0.02	0.02	0.02	0.02	0.00
Ca	0.00	0.03	0.00	0.00	0.00	0.00	0.00	0.03
#Mg	0.96	0.96	0.96	0.96	0.96	0.97	0.97	0.95

Correspondingly, Mg# is very high (0.96 – 0.97). Other elements, namely Al and Na, have very low concentration (<0.03 apfu).

Talc

Talc, present in antigorite serpentinite samples, is almost pure (Table 4), with Si = 8.00 – 8.07 apfu and Mg = 5.60 – 5.73, and low Fe = 0.17 – 0.28 apfu and Al < 0.01 apfu contents (Fig. 5). Mg# is, correspondingly, very high (0.95 – 0.97).

Chlorite

Chlorite, present in antigorite-lizardite serpentinites, has high Si (5.99 – 6.85 apfu) and Mg (9.71 – 10.27 apfu) contents, and is poor in Al (2.17 – 3.28 apfu) and Fe (0.52 – 0.87 apfu; Table 5). The contents of Cr (0.15 – 0.30 apfu) are not as high as

TABLE 3 | **Representative analyses of clinopyroxene from antigorite-lizardite serpentinites (normalized to 6 O)**

Sample	LC-97	LC-97	LC-97	LC-97	LC-97	LC-97	LC-97	LC-97	LC-97	LC-97
SiO_2	54.13	54.81	54.18	54.43	53.97	53.93	54.44	53.75	54.25	54.08
TiO_2	0.02	0.05	0.00	0.03	0.07	0.04	0.02	0.13	0.06	0.04
Al_2O_3	0.22	0.42	0.16	0.06	0.25	0.27	0.12	0.43	0.61	0.62
Cr_2O_3	0.12	0.09	0.07	0.10	0.20	0.13	0.19	0.14	0.20	0.27
Fe_2O_{3total}	1.33	1.13	1.49	1.51	1.35	1.51	1.38	1.70	1.30	1.35
MnO	0.07	0.02	0.07	0.06	0.06	0.06	0.05	0.15	0.04	0.09
MgO	18.12	18.61	17.83	17.96	18.26	18.09	18.06	18.40	18.27	18.48
CaO	25.17	24.70	25.10	25.41	24.77	24.71	25.23	24.49	24.38	24.39
Na_2O	0.14	0.28	0.21	0.11	0.20	0.18	0.15	0.18	0.27	0.23
K_2O	0.00	0.03	0.00	0.00	0.01	0.00	0.01	0.01	0.00	0.00
Sum	99.32	100.14	99.11	99.67	99.14	98.92	99.65	99.38	99.38	99.55
Si	1.97	1.98	1.98	1.98	1.97	1.97	1.98	1.96	1.97	1.97
Ti	0.00	0.00	0.00	0.00	0.00	0.00	0.00	0.00	0.00	0.00
Al	0.01	0.02	0.01	0.00	0.01	0.01	0.01	0.02	0.03	0.03
Cr	0.00	0.00	0.00	0.00	0.01	0.00	0.01	0.00	0.01	0.01
Fe^{2+}	0.04	0.03	0.04	0.04	0.04	0.04	0.04	0.05	0.04	0.04
Mn	0.00	0.00	0.00	0.00	0.00	0.00	0.00	0.01	0.00	0.00
Mg	0.99	1.00	0.97	0.97	0.99	0.99	0.98	1.00	0.99	1.00
Ca	0.98	0.96	0.98	0.99	0.97	0.97	0.98	0.96	0.95	0.95
Na	0.01	0.02	0.02	0.01	0.01	0.01	0.01	0.01	0.02	0.02
K	0.00	0.00	0.00	0.00	0.00	0.00	0.00	0.00	0.00	0.00
Sum	4.01	4.01	4.00	4.00	4.01	4.00	4.00	4.01	4.00	4.01
Wo	49.97	48.83	50.30	50.41	49.38	49.54	50.11	48.90	48.96	48.69
En	50.03	51.17	49.70	49.59	50.62	50.46	49.89	51.10	51.05	51.31
Fs	0.00	0.00	0.00	0.00	0.00	0.00	0.00	0.00	0.00	0.00

TABLE 4 | **Representative analyses of talc from antigorite-lizardite serpentinites (normalized to 20 O and 4 OH)**

Sample	LC-58	LC-58	LC-58	LC-58	LC-58	LC-58	LC-55	LC-55	LC-55	LC-55
SiO_2	62.40	62.85	62.55	63.61	62.27	61.44	62.49	62.76	61.46	62.63
TiO_2	0.05	0.04	0.00	0.02	0.02	0.04	0.02	0.05	0.05	0.01
Al_2O_3	0.04	0.02	0.04	0.03	0.00	0.01	0.01	0.04	0.00	0.01
FeO_{total}	2.49	2.34	2.20	2.12	2.10	2.33	1.61	2.41	2.60	2.11
MgO	29.54	29.54	29.70	29.88	29.82	28.63	29.61	29.54	29.38	29.57
Total	94.52	94.79	94.49	95.66	94.21	92.45	93.74	94.80	93.49	94.33
Si	8.03	8.05	8.03	8.06	8.02	8.07	8.06	8.04	8.00	8.05
Ti	0.01	0.00	0.00	0.00	0.00	0.00	0.00	0.00	0.01	0.00
Al	0.01	0.00	0.01	0.00	0.00	0.00	0.00	0.01	0.00	0.00
Fe^{2+}	0.27	0.25	0.24	0.23	0.23	0.26	0.17	0.26	0.28	0.23
Mg	5.66	5.64	5.69	5.64	5.73	5.60	5.70	5.64	5.70	5.73
Mg#	0.95	0.96	0.96	0.96	0.96	0.96	0.97	0.96	0.95	0.96

in other serpentinite bodies were chlorite formed by alteration of spinel (Jan and Windley, 1990; Proenza et al., 2004; Abu El Ela and Farahat, 2009). The high Si contents and Mg# (0.92 – 0.95) classify these chlorites as clinochlore (Bailey, 1980). Nevertheless, Al contents are lower than stoichiometric clinochlore (Fig. 5), probably as a result of intergrowth of serpentinite layers within chlorite (cf. Cressey et al., 2008).

Andradite garnet

Andradite garnet, present in antigorite-lizardite serpentinites, has Si = 2.85 – 2.93 apfu, Ca = 3.04 – 3.09 apfu, and Fe^{3+} = 1.61 – 1.88 apfu, with significant Ti contents (up to 0.32 apfu) and low concentration in Al (< 0.04 apfu), Cr (< 0.04 apfu) and Mg (< 0.06 apfu; Table 6). This type of garnet is deficient in silica as is typical of high Ti-garnets from ultramafic rocks (Müntener and Hermann, 1994 and references therein).

WHOLE ROCK GEOCHEMISTRY

Major element composition

All studied serpentinite samples have large LOI (lost on ignition) values (> 10wt%; Table 7), indicating that they are almost pure serpentinite, only sample LC-55 has higher

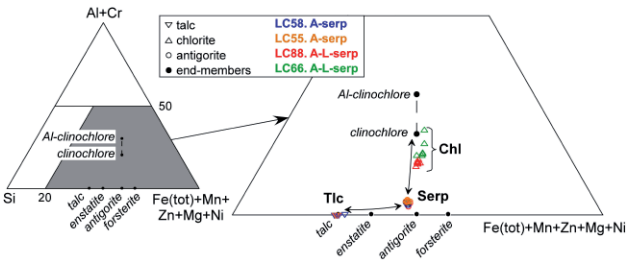

FIGURE 5 | **Atomic Si-(Al+Cr)-(Fe+Mn+Zn+Mg+Ni) diagram showing the composition of chlorite and serpentine from antigorite-lizardite serpentinites (A-L-serp) and serpentine and talc from antigorite serpentinites (A-L-serp). Representative end-members are also projected. Note that chlorites are deficient in Al.**

TABLE 5 | **Representative analyses of chlorite from antigorite-lizardite serpentinites (normalized to 20 O and 16 OH)**

Sample	LC-88	LC-88	LC-88	LC-88	LC-88	LC-88	LC-66	LC-66	LC-66	LC-66
SiO_2	34.30	34.76	34.43	34.79	34.95	36.06	31.29	32.37	32.93	34.32
TiO_2	0.03	0.02	0.01	0.02	0.00	0.00	0.07	0.05	0.01	0.05
Al_2O_3	10.57	10.64	10.95	10.57	10.06	9.67	14.55	12.95	12.36	12.50
Cr_2O_3	0.96	1.01	1.64	1.62	1.61	1.54	1.97	0.96	0.96	1.00
FeO_{total}	3.39	3.23	3.49	3.43	3.30	3.25	5.45	3.54	3.45	3.31
MnO	0.08	0.12	0.02	0.07	0.10	0.08	0.07	0.11	0.06	0.11
MgO	35.60	35.19	35.21	35.06	35.22	35.78	34.04	34.80	34.99	34.58
NiO	0.05	0.14	0.11	0.12	0.14	0.05	0.17	0.23	0.18	0.30
CaO	0.09	0.08	0.08	0.08	0.06	0.05	0.01	0.00	0.04	0.02
Total	85.07	85.19	85.94	85.76	85.44	86.48	87.62	85.01	84.98	86.19
Si	6.64	6.71	6.61	6.69	6.74	6.85	5.99	6.29	6.39	6.54
Ti	0.00	0.00	0.00	0.00	0.00	0.00	0.01	0.01	0.00	0.01
Al	2.41	2.42	2.48	2.39	2.29	2.17	3.28	2.96	2.83	2.81
Cr	0.15	0.15	0.25	0.25	0.25	0.23	0.30	0.15	0.15	0.15
Fe^{2+}	0.55	0.52	0.56	0.55	0.53	0.52	0.87	0.58	0.56	0.53
Mn	0.01	0.02	0.00	0.01	0.02	0.01	0.01	0.02	0.01	0.02
Mg	10.27	10.12	10.07	10.04	10.12	10.14	9.71	10.08	10.12	9.83
Ni	0.01	0.04	0.03	0.03	0.04	0.01	0.05	0.07	0.05	0.09
Ca	0.02	0.02	0.02	0.02	0.01	0.01	0.00	0.00	0.01	0.00
#Mg	0.95	0.95	0.95	0.95	0.95	0.95	0.92	0.95	0.95	0.95

TABLE 6 | **Representative analyses of garnet from antigorite-lizardite serpentinites (normalized to 12 O)**

Sample	LC-66	LC-66	LC-66	LC-66	LC-66	LC-66	LC-66	LC-66	LC-66
SiO_2	33.92	34.25	33.50	33.67	33.80	34.12	33.14	33.70	33.63
TiO_2	3.86	2.79	4.53	4.94	4.09	1.38	4.03	4.63	4.34
Al_2O_3	0.29	0.22	0.30	0.28	0.29	0.44	0.30	0.32	0.26
Cr_2O_3	0.27	0.05	0.08	0.40	0.42	0.54	0.37	0.29	0.34
Fe_2O_{3total}	27.02	27.59	26.17	26.12	26.55	29.21	26.89	25.52	26.36
MnO	0.07	0.04	0.02	0.08	0.13	0.05	0.09	0.06	0.07
MgO	0.33	0.33	0.46	0.41	0.32	0.14	0.36	0.39	0.38
NiO	0.00	0.00	0.00	0.00	0.00	0.00	0.00	0.00	0.17
CaO	33.25	33.27	33.41	33.30	33.45	33.26	33.13	33.77	33.70
Total	99.01	98.54	98.47	99.20	99.05	99.14	98.31	98.68	99.25
Si	2.89	2.93	2.87	2.86	2.88	2.91	2.85	2.87	2.86
Ti	0.25	0.18	0.29	0.32	0.26	0.09	0.26	0.30	0.28
Al	0.03	0.02	0.03	0.03	0.03	0.04	0.03	0.03	0.03
Cr	0.02	0.00	0.01	0.03	0.03	0.04	0.03	0.02	0.02
Fe^{3+}(*)	1.68	1.76	1.65	1.58	1.66	1.88	1.73	1.61	1.68
Fe^{2+}	0.06	0.02	0.03	0.09	0.04	0.00	0.01	0.03	0.00
Mn	0.01	0.00	0.00	0.01	0.01	0.00	0.01	0.00	0.01
Mg	0.04	0.04	0.06	0.05	0.04	0.02	0.05	0.05	0.05
Ni	0.00	0.00	0.00	0.00	0.00	0.00	0.00	0.00	0.01
Ca	3.04	3.05	3.06	3.04	3.05	3.04	3.05	3.09	3.07

(*) Calculated by stoichiometry

LOI content, suggesting alteration. Antigorite serpentinites have MgO = 35.06 – 36.32wt%, SiO_2 = 36.97 – 42.88wt%, FeO = 6.78 – 7.39wt%, Al_2O_3 = 1.49 – 2.51wt% and CaO = 0.73 – 1.93wt%. Antigorite-lizardite serpentinites have MgO = 34.72 - 37.48wt%, SiO_2 = 40.19 – 40.86wt%, FeO = 6.37 – 7.33wt%, Al_2O_3 = 2.38 – 2.93wt% and CaO = 1.12 – 3.72wt%. The Mg# in both groups is similar (89.41 – 91.00). The higher concentration of CaO in antigorite-lizardite serpentinites is in correspondence with the presence of clinopyroxene and andradite garnet in these samples while the higher Al_2O_3 is associated with the presence of chlorite.

The bulk composition of antigorite serpentinites and antigorite-lizardite serpentinites (Table 7) allow classifying the protoliths as harzburgites and lherzolites using the Ol-Opx-Cpx diagram in mole proportions (Fig. 6), and according to the fields defined by Le Maitre et al. (2002). The diagram represents the projection of bulk compositions (defined by SiO_2, Al_2O_3, FeO_{total}, MnO, MgO and CaO) in the Fo-En-Di space after projection from the exchange vectors $FeMg_{-1}$ and $FeMn_{-1}$ and the Ca-Tschermak molecule $CaAl_2SiO_6$, as calculated using software CSpace (Torres-Roldán et al., 2000). All antigorite serpentinite samples correspond to harzburgitic protoliths, while the antigorite-lizardite serpentinites suggest lherzolitic-harburgitic composition.

A comparison of the whole rock compositions of serpentinites from La Corea mélange with other regionally related ultramafic rocks are presented in Figure 7. These include the Mayari-Baracoa Ophiolite Belt (interpreted as highly refractory peridotites from an arc/back arc environment; Marchesi et al., 2006), Monte del Estado complex in Puerto Rico (interpreted as abyssal peridotite; Lewis et al., 2006b; Marchesi et al., this volume), Central Cuba serpentinites from Zaza zone and Dominican Republic serpentinites from Camú and Septentrional fault zones (interpreted as forearc peridotite; Hattori and Guillot, 2007; Saumur et al., 2010) and Dominican Republic peridotites from Río San Juan and Puerto Plata complexes (interpreted as abyssal peridotite; Saumur et al., 2010). The antigorite-lizardite serpentinite samples show compositions similar to the lherzolites of the Monte del Estado ultramafic complex and abyssal peridotites from Río San Juan and Puerto Plata complexes, Dominican Republic. Furthermore, the antigorite serpentinites have compositions similar to abyssal peridotites and with Dominican Republic serpentinites from Río San Juan and Puerto Plata complexes.

Platinum group elements composition

The studied samples have low total platinum group elements (PGE) concentrations (20-63 ppb, Table 8). The antigorite-lizardite serpentinites show similar values in all samples (35-40 ppb), while the antigorite serpentinites display somewhat larger variations (20-63 ppb). In general, all samples are characterized by poorly fractionated patters of (Os, Ir, Ru) group elements (IPGE) patterns, with relatively flat IPGE segments consistent with the

TABLE 7 | **Bulk rock chemical composition of serpentinite samples from La Corea. Group A corresponds to antigorite serpentinites and group B corresponds to antigorite-lizardite serpentinites**

Sample	LC-M-17	LC-G-4	LC55	LC56	LC58	LC66	LC88	LC97
Group	A	A	A	A	A	B	B	B
SiO_2	38.79	40.80	36.97	42.88	41.28	40.19	40.86	40.55
TiO_2	0.04	0.06	0.04	0.09	0.08	0.11	0.07	0.07
Al_2O_3	1.49	2.41	1.73	2.51	1.96	2.44	2.93	2.38
FeO_{tot}	7.03	6.96	6.78	7.39	6.98	6.82	6.37	7.33
MnO	0.11	0.11	0.16	0.10	0.09	0.13	0.13	0.14
MgO	36.32	35.52	35.06	35.31	36.00	37.48	36.17	34.72
CaO	1.20	0.68	1.93	b.d.l.	0.73	1.12	2.30	3.72
P_2O_5	0.01	0.01	0.01	0.01	0.01	0.01	0.01	0.01
LOI	13.52	12.11	17.17	10.88	12.23	11.33	10.77	10.14
Total	98.51	98.66	99.85	99.17	99.36	99.63	99.61	99.06
Mg#	0.84	0.84	0.84	0.83	0.84	0.85	0.85	0.83

LOI: Loss on ignition. b.d.l.: below detection limit

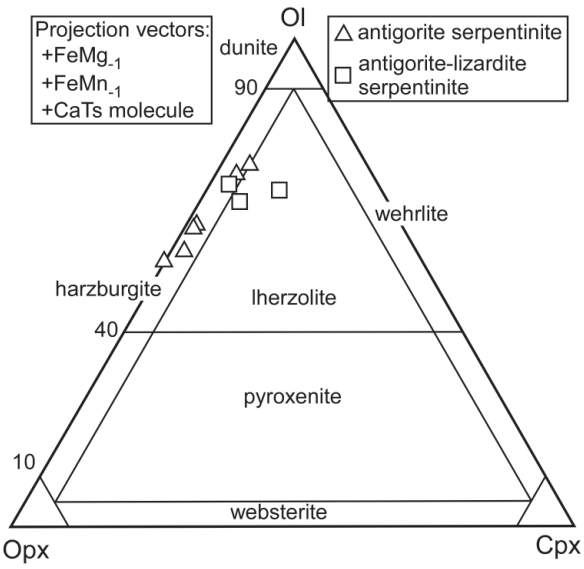

FIGURE 6 | **Calculated molar Ol-Opx-Cpx diagram for serpentinites from La Corea mélange (see text for calculation). Classification diagram from Streckeisen (1974).**

interpretation that they are all mantle residues (Fig. 8A, B). These PGE patterns are very similar to that of the primitive upper mantle (Becker et al., 2006). The composition of the studied samples are also similar to serpentinites of diverse origin (abyssal, forearc) from the Dominican Republic (Saumur et al., 2010).

In the Os versus Ir diagram (Fig. 8C) the samples show chondritic PGE abundances and weak enrichments relative to serpentinized abyssal peridotites (Snow and Reisberg, 1995; Luguet et al., 2003). The iridium contents and Ir/(Pt+Pd) ratios also indicate a mantle peridotite origin for their host protoliths (Fig. 8D). In general, the PGE distribution indicates that the PGE contents of the protoliths have not been significantly affected by metamorphism, in agreement with similar observations by Groves and Keays (1979), Prichard and Tarkian (1988), Angeli et al. (2001) and Proenza et al. (2004).

ISOCHEMICAL P-T PROJECTION

Isochemical P-T projections (pseudosections) were calculated for representative bulk-rock compositions of the two groups of serpentinites studied and the results were compared with the observed phase assemblages. The projections were computed with software PerpleX (Connolly, 2005). Thermodynamic data were taken from the internally consisted database of Holland and Powell (1998). Solid solutions considered are from Holland and Powell (1998) for olivine, from Holland and Powell (1996) for orthopyroxene and clinopyroxene, and from Holland et al. (1998) for chlorite. Talc, antigorite and tremolite were treated as ideal binary Fe-Mg solid solutions. Lizardite was not included in the calculations due to the lack of thermodynamic data for this phase. The fluid phase, assumed to be pure H_2O, is considered to be in excess. The antigorite serpentinite sample LC-58 was modeled in the CFMSH (CaO-FeO-MgO-SiO_2-H_2O) system (Fig. 9A). The bulk rock composition of this sample was slightly transformed in order to account for the Mg and Ca contents present in the carbonate phases (not considered in the calculations). The antigorite-lizardite serpentinite sample LC-97 was modeled in the system CFMASH (CaO-FeO-MgO-Al_2O_3-SiO_2-H_2O) (Fig. 9B). A small proportion of FeO_{total} was extracted to account for the presence of magnetite (not considered in the calculations).

The results of the calculations indicate a wide range of P-T conditions below ca. 500ºC for the formation of antigorite serpentinites (Fig. 9A). The predicted assemblage for these conditions is made mostly by antigorite, with minor talc, as observed in the studied samples. However, the calculated relations indicate the presence of minor tremolite, not observed in the studied samples. This is likely due to the effect of non-accounted CO_2 component and carbonate (dolomite) phases. Because these rocks are interpreted as the matrix of the subduction channel (i.e., high-T mélange formed above the subduction zone; see below), they should have followed a retrograde trajectory similar to that of the tectonic blocks of subducted oceanic material. For this reason, we have calculated mineral abundances in one point along the P-T trajectory followed by high pressure amphibolite blocks of the La Corea mélange (Blanco-Quintero et al., 2010). The results

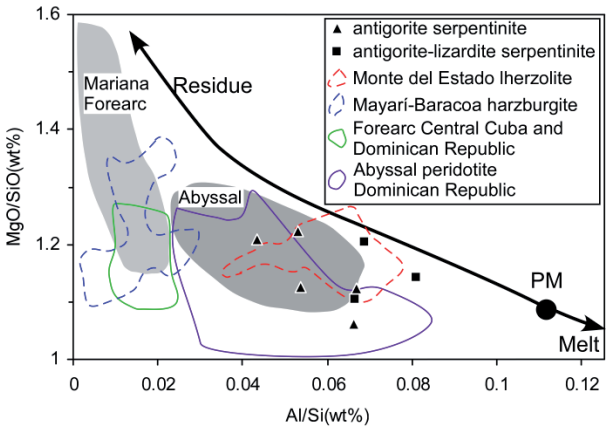

FIGURE 7 | **Weight ratios of Mg/Si versus Al/Si of serpentinite samples from La Corea mélange. Plotted for comparison are the fields of Mayarí-Baracoa harzburgites (Marchesi et al., 2006), Monte del Estado lherzolites (Marchesi et al., 2011), abyssal serpentinites from the Dominican Republic (Saumur et al., 2010), and forearc serpentinites from Central Cuba and Dominican Republic (Hattori and Guillot 2007, Saumur et al., 2010). Fields for Mariana forearc and abyssal peridotites compiled by Hattori and Guillot (2007). PM is the primitive mantle estimate of McDonough and Sun (1995).**

TABLE 8 | **Whole rock analyses of platinum group elements (PGE) of representative samples from La Corea mélange. Group A corresponds to antigorite serpentinites and group B corresponds to antigorite-lizardite serpentinites**

Samples	LC-G-4	LC-M-17	LC-55	LC-56	LC-66	LC-88	LC-97
Group	A	A	A	A	B	B	B
Ir	5	3	4	4	4	4	4
Os	4	3	4	3	3	3	4
Pd	21	7	5	7	9	13	10
Pt	18	0	10	3	5	10	10
Rh	5	2	5	2	4	3	3
Ru	10	5	10	7	10	7	9
Suma	63	20	38	26	35	40	40
IPGE	19	11	18	14	17	14	17
PPGE	44	9	20	12	18	26	23
IPGE/PPGE	0.43	1.22	0.90	1.17	0.94	0.54	0.74
Ir/(Pt+Pd)	0.13	0.43	0.27	0.40	0.29	0.17	0.20

IPGE: Os, Ir, Ru. PPGE: Rh, Pt, Pd.

indicate that the abundances of antigorite and talc are 93.63 wt% and 3.93 wt%, respectively, similar to the estimation from XRD data (see above).

The results of calculations for the antigorite-lizardite sample indicate that talc is not stable in the low temperature part of the diagram (< 600ºC; Fig 9B), as opposed to the calculations for the antigorite serpentinite sample and in agreement with observed assemblages. In addition, brucite, clinopyroxene and chlorite appear as stable phases in the low temperature field (< 400ºC), in agreement with the observed assemblages. The predicted stable coexistence of diopsidic clinopyroxene at low temperature suggests that the clinopyroxene porphyroclasts of the studied samples represent former peridotitic porphyroclasts reequilibrated during low-grade metamorphism. Since these rocks constitute tectonic blocks interpreted to have been accreted to the mélange at relatively low temperature (see below), their P-T evolution should have met the retrograde paths of the exhuming rocks of the subduction channel late during the evolution of the latter. In fact, the calculated mineral proportions at conditions appropriate for greenschist facies along the retrograde P-T path of the exotic blocks of La Corea mélange (i.e., 300ºC and 6kbar: Atg 66.46wt%, Cpx 15.20wt%, Chl 14.65wt% and Brc 3.70wt%; Fig. 9B) closely match the proportions obtained after XRD data recalculated for magnetite = 0.

DISCUSSION

The geologic setting of formation of ultramafic complexes is best determined using proxies such as the concentration of Cr, Al and Ti in Cr-spinel (Irvine, 1967; Dick and Bullen, 1984; Arai, 1992). The studied metaultramafic rocks of La Corea mélange do not preserve primary Cr-spinel, which is systematically altered to ferrian chromite or Cr-bearing magnetite. Also, no primary silicates (olivine and pyroxene) have been preserved, since diopsidic clinopyroxene of the antigorite-lizardite rocks is interpreted as metamorphic in equilibrium with antigorite. However, the fact that both types of rock have antigorite as the most abundant phase indicates a moderate temperature of serpentinization. Antigorite is the high temperature stable polymorph of the serpentine group minerals. Evans (2004) and Ulmer and Trommsdorff (1995) presented experimental results indicating antigorite stability up to 720ºC and 20kbar and 620ºC and 50kbar. These results are in agreement with formation of antigorite-bearing rocks in the subduction environment for a broad range of P-T conditions. Though the P-T conditions of formation of the studied serpentinites cannot be defined with precision, probable conditions can be deduced taking into account the dynamics of subduction channels and the evolution of high pressure exotic blocks included in the La Corea Mélange.

Dehydration of subducted altered oceanic crust and sediment from the incoming plate evolves large amounts of H_2O-fluid to the upper-plate mantle, for which models predict the possibility of partial melting at appropriate high temperature or serpentinization at low-medium temperature (e.g., Gerya et al., 2002). Subduction channels, being formed by a serpentinite matrix and HP blocks accreted from the subducting plate and/or detached from the overlying fore-arc lithosphere, may also contain exotic blocks of serpentinite formed in these environments. The strong alteration of spinel and the systematic absence of primary phases (e.g., olivine, orthopyroxene)

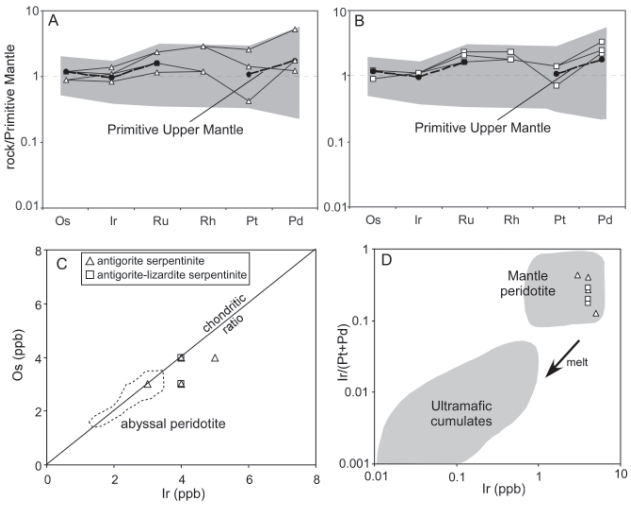

FIGURE 8 | **Primitive mantle (McDonough and Sun, 1995) normalized PGE abundances of A) antigorite serpentinite and B) antigorite-lizardite serpentinite. For reference, the composition of primitive upper mantle (PUM; Becker et al. 2006) and of abyssal and forearc serpentinites from Dominican Republic (Saumur et al., 2010) are plotted (grey fields). C) Ir versus Os diagram for samples from La Corea mélange; the field of abyssal peridotite is after compilation of Agranier et al. (2007); D) Ir versus Ir/(Pt+Pd) diagram for samples from La Corea mélange. It can be appreciated that the samples are similar to mantle peridotite and not ultramafic cumulates. The mantle peridotite and ultramafic cumulate regions (grey fields) are compiled by Hattori and Guillot (2007).**

are indications of elevated fluid fluxes and moderate temperature of formation, as indicated by the pseudosection calculations (Fig. 9). In this context, we interpret antigorite serpentinites as the deep seated serpentinitic matrix of the subduction channel formed after hydration of the boundary layer of the upper plate (harzburgitic) mantle. The bulk-rock major (Fig. 7) and PGE (Fig. 8) chemistry of this type of rock suggests a deep-seated harzburgitic protolith similar to abyssal peridotite. Harzburgites are known in abyssal and mantle wedge environments, but considering field evidence and mineralogical composition we propose that the antigorite serpentinites are derived from the hydrated mantle wedge. This interpretation implies that subduction channel serpentinites do not necessarily resemble residual harzburgites typical of fore-arcs (e.g., Mayarí-Baracoa ophiolitic complex).

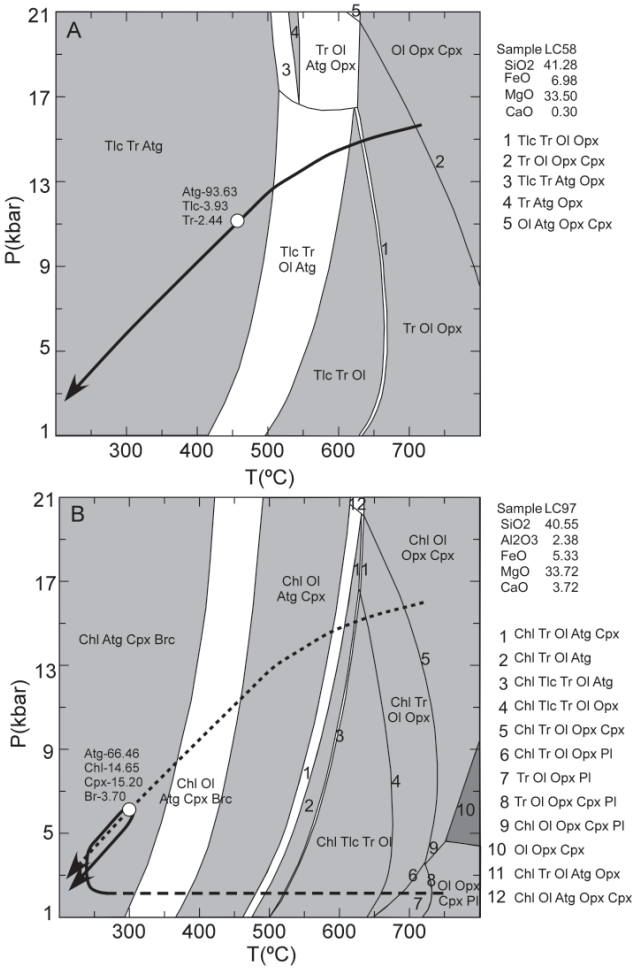

FIGURE 9 | **Isochemical P-T equilibrium phase diagram for A) antigorite serpentinite (LC58) and b) antigorite-lizardite serpentinite (LC97) calculated with Perplex. Ol: olivine, Atg: antigorite, Tlc: talc, Cpx: clinopyroxene, Opx: orthopyroxene, Chl: chlorite, Tr: tremolite, Brc: brucite. The P-T path in A) is for tectonic blocks of subducted amphibolites incorporated into the subduction channel (Blanco-Quintero et al., 2010). In B) the same P-T path is depicted with a dotted line; dashed and solid lines represent the inferred P-T paths during ocean-floor evolution of abyssal peridotites and during incorporation into the subduction channel, respectively. The calculated abundance of minerals for the inferred conditions of formation of both types of rocks is indicated.**

The antigorite serpentinites of the subduction channel would have followed a P-T path similar to that of subducted blocks accreted to the upper plate mantle. Exotic blocks of amphibolite were metamorphosed at ca. 15kbar, 700ºC, when they were accreted to the upper plate mantle (Blanco-Quintero et al., 2010). At these conditions, the calculated pseudosection for antigoritite serpentinites indicates anhydrous peridotite mineral assemblages coexisting with H_2O-fluid (i.e., hydrous peridotite; Fig. 9A). Blanco-Quintero et al. (2010) indicated that these conditions were followed by near-isobaric cooling in the accreted blocks of amphibolite, as expected after refrigeration of the subduction zone due to continued subduction (Gerya et al., 2002). Such isobaric cooling P-T path is also expected for the hydrated peridotite of the upper plate, which would hydrate (i.e., formation of tremolite and talc; Fig. 9A) due to the influx of fluids from the subducting slab. Once antigorite starts forming (ca. 650ºC, 15kbar; Fig. 9A), so does the subduction channel and rocks (both exotic tectonic blocks and hydrated metaharzburgitic matrix) begin to be exhumed. This is to be expected due to the plastic behavior of serpentinitic rocks (Gerya et al., 2002; Guillot et al., 2009) and implies that the P-T paths of the subduction channel rocks suffer an inflection, with increasing decompression upon cooling (Fig 9A). Further influx of fluids evolved from the subducting plate would allow continued hydration and the formation of almost pure antigoritite in the exhuming matrix of the subduction channel at conditions below 500ºC and 13kbar (Fig. 9A).

The lherzolitic bulk rock composition of the antigorite-lizardite serpentinites suggests a different protolith, probably an abyssal peridotite. The presence of abyssal and supra-subduction zone peridotite (protolith) rocks in subduction channels can be explained by three hypotheses. First, basaltic crust produced at slow spreading centers (Atlantic type) is normally thin or even absent, allowing abyssal peridotites to be incorporated in the subduction channel and mixed with metamafic rocks accreted from the incoming plate and hydrated ultramafic rocks of the mantle wedge. Similar rocks are described in mélanges from the Dominican Republic (Gorczyk et al., 2007, Saumur et al., 2010). Second, the preservation of abyssal-type peridotites in forearc regions has been interpreted as trapped older lithosphere that did not participate in subduction zone melting (Batanova and Sobolev, 2000). Finally, the inflow of younger abyssal lithosphere along the margins of transform-bounded trench systems is also possible, as proposed for the South Sandwich arc (Parkinson et al. 1992; Parkinson and Pearce 1998; Pearce et al. 2000).

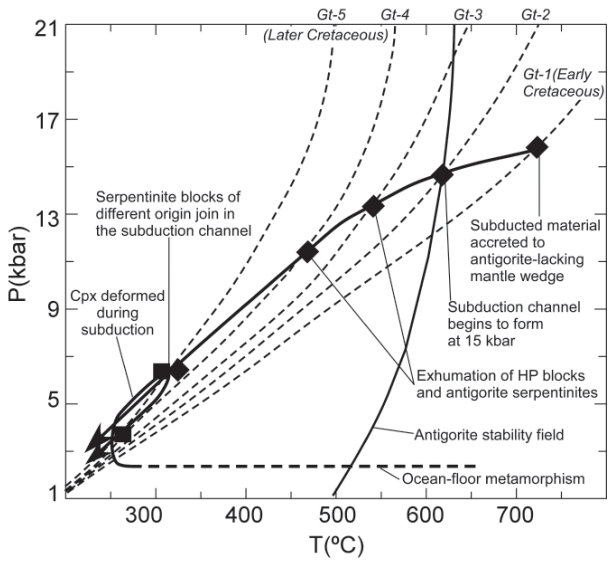

FIGURE 10 | **Schematic P-T diagram showing the model evolution of studied rocks. Dashed lines: evolving isotherms from onset of subduction to mature subduction (not scaled). Diamonds: Points along the inferred path of antigorite serpentinites (from mantle wedge to subduction channel). Squares: points along the inferred path of antigorite-lizardite serpentinites (abyssal serpentinite) during and after accretion (from the subduction channel to the mélange). The antigorite stability field corresponds to the calculation of Fig. 9A.**

The Proto-Caribbean oceanic lithosphere (Atlantic) was formed as result of breakup and disruption of Pangea during Late Jurassic - Late Cretaceous. Geological and geophysical evidence suggests a slow spreading center in the Proto-Caribbean region during the Mesozoic (e.g., Pindell et al., 2005, 2006) which may have allowed the formation of serpentinite after hydration of abyssal peridotite. Furthermore, chemical similarities among

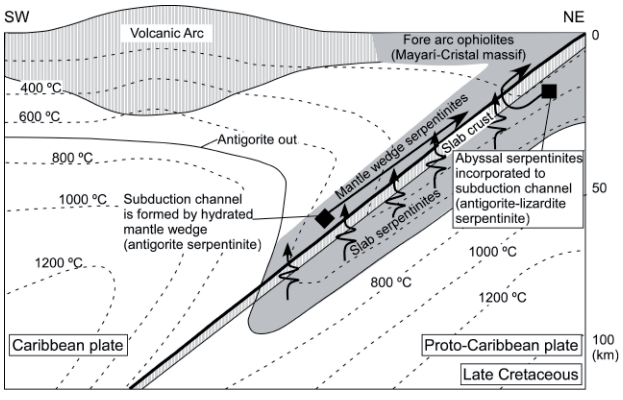

FIGURE 11 | **Schematic cross-section showing the tectonic configuration of the Caribbean region during the Cretaceous and the origin of the studied rocks. The thermal structure of the subduction zone and the stability of serpentinite is after Gerya et al. (2002; Fig. 7A) for a young plate (20Ma) after 500km of convergence.**

the antigorite-lizardite serpentinites and the Monte del Estado (Puerto Rico) ultramafic rocks (Fig. 7), interpreted as fragments of the Proto-Caribbean lithosphere (Lewis et al., 2006b; Marchesi et al., this volume), strengthen the view that the former type of rock from La Corea mélange represents fragments of the Proto-Caribbean oceanic lithosphere that escaped deep subduction. This view is consistent with the brucite, lizardite, and andradite-bearing mineral assemblages and textures of this type of rock, which suggest low temperatures of formation (Frost and Beard, 2007) in the oceanic environment and in the shallow subduction environment. Hence, the thermal evolution of this type of rocks should have encountered that of the exhuming subduction channel (mélange) at relatively low temperature and pressure. Using the P-T path of the exotic blocks of amphibolite, this should have taken place at ca. 300ºC and 5-6kbar (Fig. 9B), as indicated above.

An integrated model of evolution of serpentinites is presented in Figures 10 and 11 following the interpretations given above and those of Blanco-Quintero et al. (2010) for the exotic blocks of subducted MORB in the La Corea mélange. At the onset of subduction of young oceanic lithosphere during the Early Cretaceous (ca. 120Ma), the thermal gradient along the subduction interface was very hot. These conditions allowed the breakdown of hydrous phases from subducted hydrous oceanic lithosphere and the formation of free fluid that would flux across the mantle wedge. At relatively deep conditions, meta-MORB rocks from the incoming plate (amphibolites) were accreted to hydrous peridotitic mantle wedge. Continued subduction refrigerated the subduction system, allowing formation of hydrated metaperidotitic mantle wedge at similar depth. A serpentinitic subduction channel is formed upon reaction of liberated H_2O with the mantle wedge at conditions within the antigorite stability field (i.e., antigorite serpentinites), allowing henceforth upward flow of the rocks. This general evolution produces counter-clockwise P-T paths of accreted rocks (e.g., Wakabayashi, 1990; Gerya et al., 2002). Similar trajectories have been deduced by Krebs et al. (2008) from contemporaneous (ca. 103Ma) eclogite blocks in the Río San Juan complex (Dominican Republic), and amphibolite blocks from the Sierra del Convento mélange (115Ma; García-Casco et al., 2008a; Lázaro et al., 2009). As the subduction channel flows upward, other blocks join the mélange at shallower depths (i.e., antigorite-lizardite serpentinites). The mélange further exhumes until it is located below the forearc peridotites that could be represented by the peridotites of the Mayarí-Cristal ophiolite massif. Both the underlying forearc ophiolites and the mélange would be finally exhumed during late Cretaceous obduction, likely caused by the regional arc-platform collision event (García-Casco et al. 2008b).

CONCLUSIONS

Antigorite- and antigorite-lizardite-serpentinites in La Corea mélange (eastern Cuba) document the processes of formation of the subduction channel and accretion of abyssal peridotites. The strong alteration (i.e., serpentinization, Cr-spinel transformation) of harzburgitic and lherzolitic protholiths indicates pervasive fluid flow in all types of rock best explained if the rocks experienced hydration above a subducting plate. Antigorite serpentinites of harzburgitic protolith likely formed at depth after hydration of the mantle wedge (Caribbean lithosphere) by fluids derived from the SW-dipping subducted slab (Proto-Caribbean lithosphere). Antigorite-lizardite serpentinites of lherzolitic composition are best explained as abyssal (meta)peridotites (Proto-Caribbean lithosphere) accreted to the subduction channel developed in the Caribbean-Proto-Caribbean plate interface. Hydration of Caribbean plate mantle wedge allowed the formation and exhumation of a subduction channel during Cretaceous times until final exhumation occurred in the Late Cretaceous obduction of the supra-subduction zone Mayarí-Baracoa Ophiolite Belt and associated underlying subduction mélanges.

ACKNOWLEDGMENTS

The authors thank the constructive reviews of Robert J. Stern, Stéphane Guillot and George E. Harlow that substantially improved this paper. We appreciate financial support from Spanish MEC projects CGL2006-07384, CGL2006-08527, CGL2009-12446, CGL2009-10924 and 2009-SGR444 from the Catalan Government. This is a contribution to IGCP-546 "Subduction zones of the Caribbean". Blanco-Quintero is supported by grant AP2005-5258 from the "Programa de Formación del Profesorado Universitario" of the Spanish Ministry of Education and Science.

REFERENCES

Abu El Ela, F.F., Farahat, E.S., 2009. Neoproterozoic podiform chromitites in serpentinites of the Abu Meriewa–Hagar Dungash district, Eastern Desert, Egypt: Geotectonic implications and metamorphism. Island Arc, 19(1), 151-164. doi: 10.1111/j.1440-1738.2009.00689.x.

Adamovich, A., Chejovich, V., 1964. Principales características de la geología y de los minerales útiles de la región nordeste de la Provincia de Oriente. Revista Tecnológica, 2, 14-20.

Agranier, A., Lee, C.-T.A., Li, Z.-X.A., Leeman, W.P., 2007. Fluid-mobile element budgets in serpentinized oceanic lithospheric mantle: insights from B, As, Li, Pb, PGEs and Os isotopes in the Feather River Ophiolite, California. Chemical Geology, 245, 230-241.

Angeli, N., Fleet, M.E., Thibault, Y., Candia, M.A.F., 2001. Metamorphism and PGE-Au content of chromitite from the Ipanema mafic/ultramafic Complex, Minas Gerais, Brazil. Mineralogy and Petrology, 71, 173-194.

Arai, S., 1992. Chemistry of chromian spinel in volcanic rocks as a potential guide to magma chemistry. Mineralogical Magazine, 56, 173-784.

Bailey, S.W., 1980. Summary of recommendations of AIPEA nomenclature committee. Clay Minerals, 15, 85-93.

Batanova, V.G., Sobolev, A.V., 2000. Compositional heterogeneity in subduction-related mantle peridotites, Troodos massif, Cyprus. Geology, 28, 55-58.

Becker, H., Horan, M.F., Walker, R.J., Gao, S., Lorand, J.P., Rudnick, R.L., 2006. Highly siderophile element compositions of the Earth's primitive mantle. Geochimica et Cosmochimica Acta, 70, 4528-4550.

Blanco-Quintero, I., García-Casco, A., Rojas Agramonte, Y., Rodríguez Vega, A., Lázaro, C., Iturralde-Vinent, M.A., 2010. Metamorphic evolution of subducted hot oceanic crust, La Corea mélange, Cuba. American Journal of Science, 310, 889-915.

Boiteau, A., Michard, A., Saliot, P., 1972. Métamorphisme de haute pression dans le complexe ophiolitique du Purial (Oriente, Cuba). Comptes Rendus de l'Académie des Sciences, Série D, 274, 2137-2140.

Capitani, G., Mellini, M., 2004.The modulated crystal structure of antigorite: The m = 17 polysome. American Mineralogist, 89, 147-158.

Capitani, G., Mellini, M., 2006. The crystal structure of a second antigorite polysome (m=16), by single-crystal synchrotron diffraction. American Mineralogist, 91, 394-399.

Chan, T.K., Finch, I.J., 2001. Determination of platinum-group elements and gold by inductively coupled plasma mass spectrometry. In: Australian Platinum Conference, Perth, Western Australia.

Cobiella, J., Campos, M., Boiteau, A., Quintas, F., 1977. Geología del flanco sur de la Sierra del Purial. Revista La Minería de Cuba, 3, 54-62.

Connolly, J.A.D., 2005. Computation of phase equilibria by linear programming: a tool for geodynamic modeling and its application to subduction zone decarbonation. Earth and Planetary Science Letters, 236, 524-541.

Cressey, G., Cressey, B.A., Wicks, F.J., 2008. The significance of the aluminium content of a lizardite at the nanoscale: the role of clinochlore as an aluminium sink. Mineralogical Magazine, 72, 817-825.

D'Antonio, M.D., Kristensen, M.B., 2004. Hydrothermal alteration of oceanic crust in the West Philippine Sea Basin (Ocean Drilling Program Leg 195, Site 1201): inferences from a mineral chemistry investigation. Mineralogy and Petrology, 83(1-2), 87-112. doi: 10.1007/s00710-004-0060-6.

Dick, H.J.B., Bullen, T., 1984. Chromian spinel as a petrogenetic indicator in abyssal and alpine-type peridotites and spatially associated lavas. Contributions to Mineralogy and Petrology, 86, 54-76.

Escartín, J., Andreani, M., Hirth, G. Evans, B., 2008. Relationships between the microstructural evolution and the rheology of talc

at elevated pressures and temperatures. Earth and Planetary Science Letters, 268, 463-475.

Evans, B.W., 2004. The serpentinite multisystem revisited: Chrysotile is metastable. International Geology Review, 46, 479-506.

Fonseca, E., Zelepugin, V.N., Heredia, M., 1985. Structure of the ophiolite association of Cuba. Geotectonics, 19, 321-329.

Frost, B.R., Beard, J.S., 2007. On silica activity and serpentinization. Journal of Petrology, 48, 1351-1368.

García-Casco, A., Torres-Roldán, R.L., Iturralde-Vinent, M.A., Millán, G., Núñez Cambra, K., Lázaro, C., Rodríguez Vega, A., 2006. High pressure metamorphism of ophiolites in Cuba. Geologica Acta, 4(1-2), 63-88.

García-Casco, A., Lázaro, C., Torres-Roldán, R.L., Núñez Cambra, K., Rojas Agramonte, Y., Kröner, A., Neubauer, F., Millán, G., Blanco-Quintero, I., 2008a. Partial melting and counterclockwise P-T path of subducted oceanic crust (Sierra del Convento mélange, Cuba). Journal of Petrology, 49, 129-161.

García-Casco, A., Iturralde-Vinent, M.A., Pindell, J., 2008b. Latest Cretaceous collision/accretion between the Caribbean Plate and Caribeana: Origin of metamorphic terranes in the Greater Antilles. International Geology Review, 50, 781-809.

Gervilla, F., Proenza, J.A., Frei, R., González-Jiménez, J.M., Garrido, C.J., Melgarejo, J.C., Meibom, A., Díaz-Martinez, R., Lavaut, W., 2005. Distribution of platinum-group elements and Os isotopes in chromite ores from Mayarí-Baracoa Ophiolitic Belt (eastern Cuba). Contributions to Mineralogy and Petrology, 150, 589-607.

Gerya, T.V., Stoeckhert, B., Perchuk, A.L., 2002. Exhumation of high-pressure metamorphic rocks in a subduction channel—a numerical simulation. Tectonics, 21, 1056. doi:10.1029/2002TC001406.

Gorczyk, W., Guillot, S., Gerya, T.V., Hattori, K.H., 2007. Asthenospheric upwelling, oceanic slab retreat and exhumation of UHP mantle rocks: Insights from Greater Antilles. Geophysical Research Letters, 34, L21309, 5pp. doi: 10.1029/2007GL031059.

Groves, D.I., Keays, R.R., 1979. Mobilisation of ore-forming elements during alteration of dunites, Mt Keith-Betheno, Western Australia. The Canadian Mineralogist, 17, 373-389.

Guillot, S., Hattori, K., Agard, P., Schwartz, S., Vidal, O., 2009. Exhumation processes in oceanic and continental subduction contexts: a review. In: Lallemand, S., Funiciello F. (eds.). "Subduction Zone Dynamics". Springer-Verlag Berlin Heidelberg, 175-204. doi: 10.1007/978-3-540-87974-9.

Hattori, K.H., Guillot, S., 2007. Geochemical character of serpentinites associated with high- to ultrahigh-pressure metamorphic rocks in the Alps, Cuba, and the Himalayas: Recycling of elements in subduction zones. Geochemistry, Geophysics, Geosystems, 8, Q09010. doi:10.1029/2007GC001594.

Holland, T.J.B., Powell, R., 1996. Thermodynamics of order–disorder in minerals.2. Symmetric formalism applied to solid solutions. American Mineralogist, 81, 1425-1437.

Holland, T.J.B., Powell, R., 1998. An internally consistent thermodynamic data set for phases of petrological interest. Journal of Metamorphic Geology, 16, 309-343.

Holland, T.J.B., Baker, J., Powell, R., 1998. Mixing properties and activity-composition relationships of chlorites in the system MgO-FeO-Al_2O_3-SiO_2-H_2O. European Journal of Mineralogy, 10, 395-406.

Irvine, T.N., 1967. Chromian spinel as a petrogenetic indicator; Part II, Petrologic applications. Canadian Journal of Earth Sciences, 4, 71-103.

Iturralde-Vinent, M.A., 1998. Sinopsis de la Constitución Geológica de Cuba. Acta Geologica Hispanica, 33, 9-56.

Iturralde-Vinent, M.A., Díaz Otero, C., Rodríguez Vega, A., Díaz Martínez, R., 2006. Tectonic implications of paleontologic dating of Cretaceous-Danian sections of Eastern Cuba. Geologica Acta, 4(1-2), 89-102.

Iturralde-Vinent, M.A., Díaz Otero, C., García-Casco, A., Van Hinsbergen, D.J.J., 2008. Paleogene Foredeep Basin Deposits of North-Central Cuba: A Record of Arc-Continent Collision between the Caribbean and North American Plates. International Geology Review, 50, 863-884.

Jan, M.Q., Windley, B.F., 1990. Chromian spinel–silicate chemistry in ultramafic rocks of the Jijal Complex, Northwest Pakistan. Journal of Petrology, 31, 667-715.

Krebs, M., Maresch, W.V., Schertl, H.P., Baumann, A., Draper, G., Idleman, B., Münker, C., 2008. The dynamics of intra-oceanic subduction zones: A direct comparison between fossil petrological evidence (Rio San Juan Complex, Dominican Republic) and numerical simulation. Lithos, 103, 106-137.

Kretz, R., 1983. Symbols for rock-forming minerals. American Mineralogist, 68, 277–279.

Lázaro, C., García-Casco, A., 2008. Geochemical and Sr-Nd isotope signatures of pristine slab melts and their residues (Sierra del Convento mélange, eastern Cuba. Chemical Geology, 255, 120-133.

Lázaro, C., García-Casco, A., Neubaurer, F., Rojas-Agramonte, Y., Kröner, A., Iturralde-Vinent, M.A., 2009. Fifty-five-million-year history of oceanic subduction and exhumation at the northern edge of the Caribbean plate (Sierra del Convento mélange, Cuba. Journal of Metamorphic Geology, 27, 19-40.

Le Maitre, R.W., Streckeisen, A., Zanettin, B., Le Bas, M.J., Bonin, B., Bateman, P., Bellieni, G., Dudeck, A., Efremova, S., Keller, J., Lameyre, J., Sabine, P.A., Schmid, R., Sorensen, H., Woolley, A.R., 2002. Igneous rocks. A Classification and Glossary of Terms. Recommendations of the International Union of Geological Sciences Subcommission on the Systematics of Igneous Rocks. Cambridge, 2nd Edition, Cambridge University Press, 252pp.

Lewis, J.F., Draper, G., Proenza, J.A., Espaillat, J., Jimenez, J., 2006a. Ophiolite-Related Ultramafic Rocks (Serpentinites) in the Caribbean Region: A Review of their Occurrence, Composition, Origin, Emplacement and Ni-Laterite Soils Formation. Geologica Acta, 4(1-2), 237-263.

Lewis, J.F., Proenza, J.A., Jolly, W.T., Lidiak, E.G., 2006b. Monte del Estado (Puerto Rico) and Loma Caribe (Dominican

Republic) peridotites: A look at two different Mesozoic mantle sections within northern Caribbean region. Geophysical Research Abstracts, 8, A-08798.

Li, X.-P., Rahn, M., Bucher, K., 2004. Serpentinites of the Zermatt-Saas ophiolite complex and their texture evolution. Journal of Metamorphic Geology, 22, 159-177.

Luguet, A., Lorand, J.P., Seyler, M., 2003. Sulfide petrology and highly siderophile element geochemistry of abyssal peridotites: a coupled study of samples from the Kane Fracture Zone (45 degrees W23 degrees 20 N, MARK Area, Atlantic Ocean). Geochimica et Cosmochimica Acta, 67(8), 1553-1570.

Marchesi, C., Garrido, C.J., Godard, M., Proenza, J.A., Gervilla, F., Blanco-Moreno, J., 2006. Petrogenesis of highly depleted peridotites and gabbroic rocks from the Mayarí-Baracoa Ophiolitic Belt (eastern Cuba). Contributions to Mineralogy and Petrology, 151, 717-736.

Marchesi, C., Garrido, C.J., Bosch, D., Proenza, J.A., Gervilla, F., Monié, P., Rodríguez-Vega, A., 2007. Geochemistry of Cretaceous magmatism in eastern Cuba: recycling of North American continental sediments and implications for subduction polarity in the Greater Antilles Paleo-arc. Journal of Petrology, 48, 1813-1840.

Marchesi, C., Jolly, W.T., Lewis, J.F., Garrido, C.J., Proenza, J.A., Lidiak, E.G., 2011. Petrogenesis of fertile mantle peridotites from the Monte del Estado massif (southwest Puerto Rico): a preserved section of Proto-Caribbean lithospheric mantle? Geologica Acta, 9(3-4), 289-306.

McDonough, W.F., Sun, S.-S., 1995. The composition of the Earth. Chemical Geology, 120, 223-254.

Mellini, M., Trommsdorff, V., Compagnoni, R., 1987. Antigorite polysomatism: behaviour during progressive metamorphism. Contributions to Mineralogy and Petrology, 97, 147-155.

Mellini, M., Viti, C., 1994. Crystal structure of lizardite-1T from Elba, Italy. American Mineralogist, 79, 1194-1198.

Millán, G., Somin, M.L., Díaz, C., 1985. Nuevos datos sobre la geología del macizo montañoso de la Sierra del Purial, Cuba Oriental. Reporte de Investigación del Instituto de Geología y Paleontología, 2, 52-74.

Morimoto, N., Fabries, J., Ferguson, A.K., Ginzburg, I.V., Ross, M., Seifeit, F.A., Zussman, J., 1989. Nomenclature of pyroxenes. Canadian Mineralogist, 27, 143-156.

Müntener, O., Hermann, J., 1994. Titanian andradite in a metapyroxenite layer from the Malenco ultramafics (Italy) – implications for Ti-mobility and low-oxygen fugacity. Contributions to Mineralogy and Petrology, 116, 156-168.

Nuñez Cambra, K.E., García-Casco, A., Iturralde-Vinent, M.A., Millán, G., 2004. Emplacement of the ophiolite complex in Eastern Cuba. Florence, Proceedings of the 32nd International Geological Congress, Session G20.11, Caribbean Plate Tectonics, CD-Room.

O'Hanley, D.S., 1996. Serpentinites Records of Tectonic and Petrological History. Oxford, Oxford University Press, 290pp.

Padrón-Navarta, J.A., Hermann, J., Garrido, C.J., López Sánchez-Vizcaíno, V., Gómez-Pugnaire, M.T., 2010. An experimental investigation of antigorite dehydration in natural silica-enriched serpentinite. Contributions to Mineralogy and Petrology, 159, 25-42.

Parkinson, I.J., Pearce, J.A., 1998. Peridotites of the Izu-Bonin-Mariana forearc (ODP Leg 125) evidence for mantle melting and melt–mantle interactions in a suprasubduction zone setting. Journal of Petrology, 39, 1577-1618.

Parkinson, I.J., Pearce, J.A., Thirwall, M.F., Johnson, K.T.M., Ingram, G., 1992. Trace element geochemistry of peridotites from the Izu-Bonin-Mariana forearc, Leg 125. In: Fryer, P., Pearce, J.A., Stokking, L.B. (eds.). Proceedings of ODP science results. Ocean Drilling Program, College Station, 125, 487-506.

Pearce, J.A., Barker, P.F., Edwards, S.J., Parkinson, I.J., Leat, P.T., 2000. Geochemistry and tectonic significance of peridotites from the South Sandwich arc-basin system, south Atlantic. Contributions to Mineralogy and Petrology, 139, 36-53.

Pindell, J.L., Kennan, L., Maresch, W.V., Stanek, K.P., Draper, G., Higgs, R., 2005. Plate-kinematics and crustal dynamics of circum-Caribbean arc–continent interactions: Tectonic controls on basin development in Proto-Caribbean margins. In: Avé Lallemant, H.G., Sisson, V.B. (eds.). Caribbean–South American Plate Interactions, Venezuela. Geological Society of America, 394 (Special Papers), 7-52.

Pindell, J.L., Kennan, L., Stanek, K.P., Maresch, W.V., Draper, G., 2006. Foundations of Gulf of Mexico and Caribbean evolution: eight controversies resolved. Geologica Acta, 4(1-2), 303-341.

Prichard, H.M., Tarkian, M., 1988. Platinum and palladium minerals from two PGE-rich localities in the Shetland Ophiolite Complex. The Canadian Mineralogist, 26, 979-990.

Proenza, J., Gervilla, F., Melgarejo, J.C., Bodinier, J.L., 1999. Al- and Cr rich chromitites from the Mayarí-Baracoa Ophiolitic Belt (eastern Cuba): consequence of interaction between volatile-rich melts and peridotite in suprasubduction mantle. Economic Geology, 94, 547-566.

Proenza, J., Alfonso, J., Melgarejo, J.C., Gervilla, F., Tritlla, J., Fallick, A.E., 2003. D, O and C isotopes in podiform chromitites as fluid tracers for hydrothermal alteration processes of the Mayarí-Baracoa Ophiolitic Belt, eastern Cuba. Journal of Geochemical Exploration, 78-79, 117-122.

Proenza, J.A., Ortega-Guitiérrez, F., Camprubí, A., Tritlla, J., Elías-Herrera, M., Reyes-Salas, M., 2004. Paleozoic serpentinite-enclosed chromitites from Tehuitzingo (Acatlán) Complex, southern Mexico): a petrological and mineralogical study. Journal of South American Earth Sciences, 16, 649-666.

Proenza, J.A., Díaz-Martínez, R., Iriondo, A., Marchesi, C., Melgarejo, J.C., Gervilla, F., Garrido, C.J., Rodríguez-Vega, A., Lozano-Santacruz, R., Blanco-Moreno, J.A., 2006. Primitive Cretaceous island-arc volcanic rocks in eastern Cuba: the Téneme Formation. Geologica Acta, 4(1-2), 103-121.

Saumur, B-M., Hattori, K.H., Guillot, S., 2010. Contrasting origins of serpentinites in a subduction complex, northern

Dominican Republic. Geological Society of America Bulletin, 122, 292-304.

Snow, J.E., Reisberg, L., 1995. Os isotopic systematics of theMORB mantle: results from altered abyssal peridotites. Earth and Planetary Science Letters, 136(3-4): 723-733.

Somin, M.L., Millán, G., 1981. Geology of the Metamorphic Complexes of Cuba (in Russian). Moscow, Nauka, 219pp.

Streckeisen, A.L., 1974. Classification and Nomenclature of Plutonic Rocks. Recommendations of the IUGS Subcommission on the Systematics of Igneous Rocks. Geologische Rundschau, 63, 773-785.

Torres-Roldán, R.L., García-Casco, A., García-Sánchez, P.A., 2000. CSpace: An integrated workplace for the graphical and algebraic analysis of phase assemblages on 32-bit Wintel platforms. Computers and Geosciences, 26, 779-793.

Ulmer, P., Trommsdorff, V., 1995. Serpentine stability to mantle depths and subduction-related magmatism. Science, 268, 858-861.

Wakabayashi, J., 1990. Counterclockwise P-T-t paths from amphibolites, Franciscan Complex, California: Relics from the early stages of subduction zone metamorphism. Journal of Geology, 98, 657-680.

Wicks, F.J., Whittaker, E.J.W., 1977. Serpentine textures and serpentinization. The Canadian Mineralogist, 15, 459-488.

Manuscript received November 2010;
revision accepted January 2011;
published Online March 2011.